Ecological Engineering 47 (2012) 165–173

Contents lists available at SciVerse ScienceDirect

Ecological Engineering

journal homepage: www.elsevier.com/locate/ecoleng

Validation of predictive heat and mass transfer green roof model with extensive green roof field data

Paulo Cesar Tabares-Velasco[a,*], Mingjie Zhao[a], Nicole Peterson[b,1], Jelena Srebric[a], Robert Berghage[b]

[a] Department of Architectural Engineering, The Pennsylvania State University, United States
[b] Department of Horticulture, The Pennsylvania State University, United States

ARTICLE INFO

Article history:
Received 9 November 2011
Received in revised form 5 June 2012
Accepted 22 June 2012

Keywords:
Green roof
Energy simulation
Model validation
Heat and mass transfer

ABSTRACT

Green roof technology has been adopted in the United States as a specialized roofing system and as a sustainable technology capable of saving energy. Most of the previous thermal performance models for green roofs have had the main goal of quantifying these energy savings. However, until recently, none of the models had been fully validated with laboratory and experimental data including both heat flux and surface temperature data. A recently developed green roof thermal performance model was validated with detailed experimental data from a new experimental apparatus called a Cold Plate, which is specifically designed and built for that purpose. In order to further examine the accuracy of the model, this paper describes the dynamic validation of the model using field data from a green roof installed on a commercial roof in Chicago. The dynamic validation consists of comparing substrate surface temperature, heat flux through the roof, and net radiation. The validated results show that the green roof thermal model predicts the heat and mass transfer appropriately as long as the long-wave radiation data from a weather station are used to reduce a possible bias resulting from the sky condition.

1. Introduction

Extensive green roofs are a technology that was originally promoted in Europe several decades ago. Their introduction into the United States started during the last decade, and has grown 16–50% annually during the last 5 years (Miller and Narejo, 2005; Johnston, 2007; Peck, 2011). A green roof is a specialized roofing system that supports plant life and usually consists of: (1) plants that are drought resistant, (2) a light substrate or engineered soil that holds enough nutrients and water, and (3) an optional filter and drainage layer to transport the excess rainwater off the roof. Studies on green roofs have focused on storm water runoff (Justyna, 2010; Gregoire and Clausen, 2011), plant survival and performance under different weather conditions (MacIvor and Lundholm, 2011), alternative substrate materials (Molineux et al., 2009) and thermal performance or energy modeling. Early energy modeling efforts (Nayak et al., 1982) preceded more detailed models that have been developed within the last 10–15 years. Recent studies developed the green roof models primarily to quantify the energy savings on a green roof (He, 2010). Table 1 summarizes features of the most detailed models capable of calculating energy savings.

All of the models presented in Table 1 use an overall energy balance around the green roof. Furthermore, some of the models also carry out an additional mass balance. Other models separate or discretize the green roof into several layers and calculate an energy balance in each layer. This discretization potentially increases the accuracy of a model, but it also increases the number of equations needed to solve the problem. Only one of the models accounts for changes in the water content of the substrate due to evapotranspiration and precipitation (Lazzarin et al., 2005; Sailor 2008). Evapotranspiration is a complex physical phenomenon that combines substrate water evaporation and plant transpiration. In the models shown in Table 1, evapotranspiration is mainly calculated by the vapor pressure deficit (VPD) method (Nayak et al., 1982; Del Barrio, 1998; Lazzarin et al., 2005; Alexandri and Jones, 2007; Sailor, 2008; Tabares-Velasco and Srebric, 2009a, 2012). Nevertheless, each study uses different resistance functions that represent the actual plants and substrate resistance to water movement inside of the plant leaves and substrate.

These models typically include solutions to the unsteady heat conduction equation, although some use quasi-steady state conditions. The common assumptions shown in Table 1 are:

1. Plants and green roof substrate are horizontally homogeneous,
2. Heat and mass transfer are vertical, while horizontal fluxes are negligible,
3. Air beneath stomata is saturated,

* Corresponding author. Present address: National Renewable Energy Lab, 1617 Cole Blvd. MS 5202, Golden, CO 80401, United States. Tel.: +1 303 384 7591.
E-mail address: paulo.tabares@nrel.gov (P.C. Tabares-Velasco).
[1] Present address: Atelier Ten, 45 East 20th Street, 4th Floor, New York, NY 10003, United States.

0925-8574/$ – see front matter © 2012 Elsevier B.V. All rights reserved.
http://dx.doi.org/10.1016/j.ecoleng.2012.06.012

Table 1
Comparison of heat and mass transfer functions used in green roof models.

Study	Balance	Evapotranspiration (ET)	Assumptions[a]	Roof discretization	Validation
Tabares-Velasco and Srebric (2011)	Heat and mass	Vapor pressure differential (VPD) and stomatal resistance model	Quasi-steady state conditions	Plants and substrate	Quasi-steady state: ET, conductive heat flux, convection, plant and substrate surface temperature
Sailor (2008)	Heat and mass	VPD and stomatal resistance model	1, 2, 4, 5	Two substrate layers, plants, air around plants	Surface temperature
Alexandri and Jones (2007)	Heat and mass (no rain)	VPD and stomatal resistance model	1–8	Multiple nodes	Temperature and Stomata resistance
Takebayashi and Moriyama (2000)	Heat and mass (no rain)	Evaporative efficiency and humidity difference	Evaporative efficiency	No	Temperature and volumetric water content (VWC)
Gaffin et al. (2005)	Heat	Bowen ratio	1, 2–5, 7, 9	No	Surface temperature
Lazzarin et al. (2005)	Heat and mass	VPD and wind correlation	1, 2, 4, 6	Multiple modes	Evapotranspiration
Del Barrio (1998)	Heat and mass (no rain, constant VWC)	VPD and stomatal resistance model	1, 2, 4, 6, 7	Plants, soil, roof	N/A
Nayak et al. (1982)	Heat	VPD and wind correlation	1, 4	Plants and soil	N/A

[a] Assumptions numbers are described below Table 1.

4. Biochemical reactions of plants (photosynthesis) result in negligible heat fluxes,
5. Conduction heat transfer in plants is negligible,
6. Plants are well irrigated, healthy, and in the fully grown stage,
7. Water distribution within the canopy is homogeneous,
8. Plant–soil layer is free from mulch, and
9. Green roof substrate is completely covered by plants

The most common assumptions are horizontally homogeneous roof materials and vertical heat and mass fluxes. These two assumptions significantly simplify models by limiting the problem to one dimension. The next three assumptions, numbered as 3, 4, and 5, simplify heat transfer processes related to plant biology because plants are very complex systems and their role in the overall energy balance is minimal. Assumptions 6 and 7 are also commonly used and presume that the volumetric water content (VWC) in the substrate does not change with time, as the green roof is irrigated. As a result, there are no changes in the thermal properties of the substrate, or in the canopy resistance due to water stress. These assumptions simplify the green roof modeling because the mass balance is easier to implement by eliminating the need to calculate the water losses due to drainage and evaporation, as well as the water gains due to the precipitation. In reality, plants are watered during the establishment period, typically during the first year of planting. Beyond this initial growth phase, irrigation depends on the local rainfall and weather, and in some cases plants may not need supplemental irrigation at all (Snodgrass, 2006). Thus, variations in the water content in the substrate and plant coverage are expected for typical extensive green roofs and will be implemented in modeling efforts in the present study. Assumption 8 implies that the green roof substrate is primarily responsible for the substrate evaporation without any attenuation of the vapor transfer to the environment. Finally, assumption 9 is very common because LAI (leaf area index) and plant coverage are unknown in many practical applications, although 100% plant coverage is not common.

Until recently, none of the models had been fully validated with experimental data including both heat fluxes and surface temperatures. This is due to the difficulty of performing experiments in the field, as previously described in other field study (Perino and Serra, 2003). Therefore, a new experimental apparatus was designed and built to measure important heat and mass transfer processed between the substrate, plants, sky, and surrounding air (Tabares-Velasco and Srebric, 2011). The new apparatus, called "Cold Plate", was installed inside a full-scale environmental chamber to allow for controlled environmental conditions and the use of laboratory-rate instrumentation. "Cold Plate" apparatus allows for simultaneous measurement of evapotranspiration, radiation, heat flux through the green roof, spectral properties of the plants and substrate to surface temperature of plants and substrate (Tabares-Velasco and Srebric, 2011). The data collected allowed for dynamic and quasi-steady-state comparisons of thermal performance for a green roof without plants and with plants (Tabares-Velasco and Srebric, 2009a,b). This comparison showed that plants play an important role in modulating and diverting heat fluxes off the roof. More importantly, these data sets allowed for a detailed verification and validation of a green roof model in quasi-steady-state conditions (Tabares-Velasco and Srebric, 2012). However, this heat and mass transfer model was only validated in quasi-steady-state conditions. In order to assure the accuracy of the model, this paper describes the dynamic validation of the model based on the field data from a green roof installed on a commercial building in Chicago during summer weather conditions.

2. Description of experimental green roof

The instrumented green roof is located in Chicago, Illinois. The total area of the roof is about 14,000 m^2 and about half of that roof area is covered with a green roof. A sketch of the green roof system and allocation of instrumentation is shown in Fig. 1. From top to bottom, the installed green roof consists of: (1) a plant layer of mixed Sedum species, (2) 7.5 cm substrate layer, (3) two layers of polypropylene fabric layers, (4) 2.5 cm of thick foam drainage/protection board made from chunks of recycled closed cell polystyrene, and (5) 0.2 cm PVC waterproof membrane layer. The substrate used was based on expanded clay and has a dry bulk density of 650 kg/m^3, bulk density at the maximum water-holding

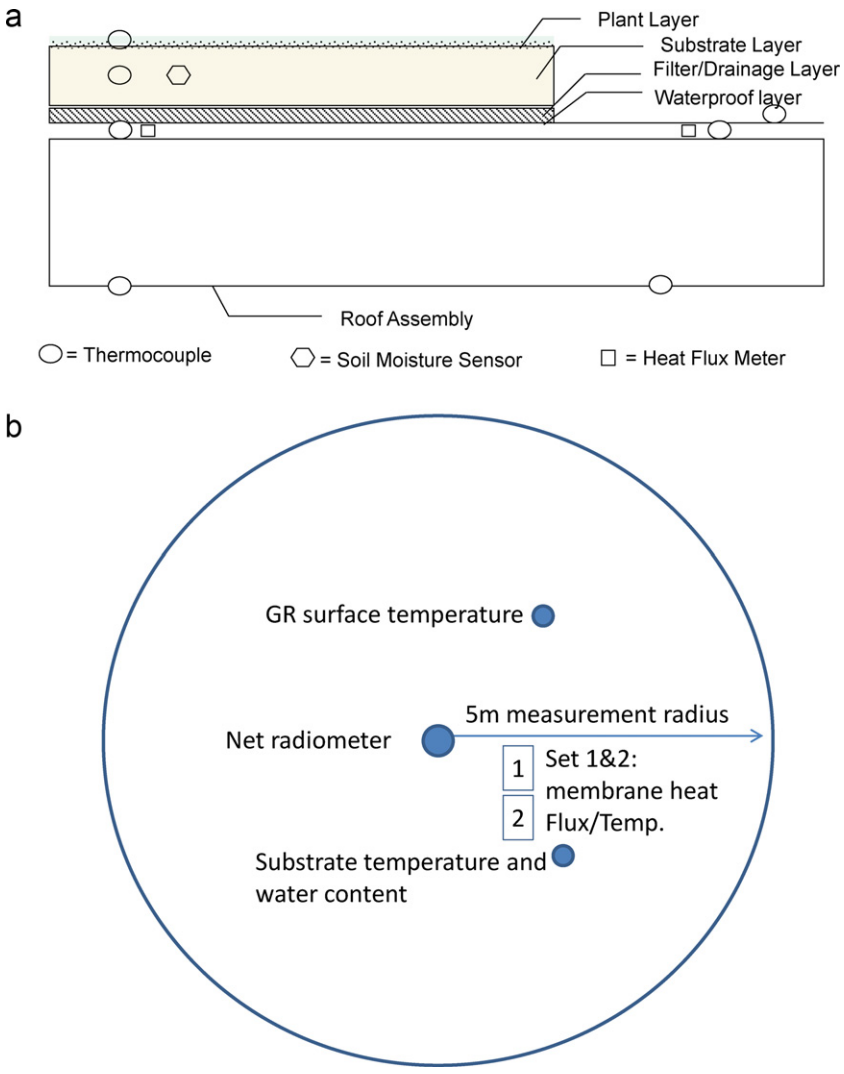

Fig. 1. Green roof vertical cross-section (a) and top view (b) indicating allocation of temperature, moisture and heat flux sensors.

capacity of 1130 kg/m^3, and a maximum volumetric water-holding capacity of 49.6%. Overall, rest of the layers under the green roof was:

- Steel deck
- 0.6 cm gypsum board
- 10 cm of insulation (R = 20, nominal)
- 0.6 cm gypsum board
- 0.6 cm felt protection layer

Additionally, the green roof was instrumented with temperature, heat flux, water content sensors and a weather station recording outdoor weather data every 1 min and averaging every 15 min. Fig. 1a and b shows the location of the sensors. Overall, the variables measured on-site are shown in Table 2.

As shown in Fig. 1b, two identical instrumentation sets that measured temperature and heat flux underneath the waterproofing membrane were installed less than 1 m apart. The rest of the green roof temperature and water content sensors were within a 5 m radius. Thus, each set was not aligned vertically due to logistic problems. Therefore, the membrane heat fluxes and surface temperatures presented in this study represent the average readings from the two sensors. Overall, there was no significant variation among the two sets of sensors.

In addition to the thermal instrumentation, the water content sensors measured the volumetric water content (VWC) in the substrate. They were originally set up with the manufacturer's calibration equation that is based on a broad sample of soils shown in Eq. (1) (Campbell Scientific, 2009). However, green roof substrate is not, by definition, soil. Laboratory experiments with a similar green roof substrate revealed that the manufacturer's equation tends to underestimate the actual water content of the substrate. Thus, this study uses a new calibration equation as shown in Eq. (2) (Tabares-Velasco and Srebric, 2012):

$$\mathrm{VWC_{CS}} = 0.0283_{\tau} - 0.4677 \quad (1)$$

$$\mathrm{VWC_{new}} = 0.05_{\tau} - 0.7479 \quad (2)$$

In Eqs. (1) and (2), τ represents the raw output from the water content sensor. The concept of volumetric water content can be explained further by looking into its definition and the equilibrium between the soil, air, and water in a particular volume. The total volume is equal to the combination of the volume of the solids, air, and water. This can be described with the following equation:

$$V_{\mathrm{total}} = V_{\mathrm{soil}} + V_{\mathrm{air}} + V_{\mathrm{H_2O}} \quad (3)$$

Table 2
Specifications of instrumentation used.

Sensor	Measured variable	Location	Accuracy	Model
Heat flux transducer	Heat flux through the green roof	Under green roof waterproof membrane	±5%	F-005-4 heat Flow sensor w/integrated Thermocouples
Net radiometer	Net radiation	1.2 m above green roof	±10%	NR-LITE
Thermocouple	Several surface temperatures	GR surface temperature GR waterproof membrane temperature	±0.5 °C	Type T
Water content reflectometer	Substrate volumetric water content	Middle of substrate depth	2.5% standard calibration	CS616-L water Content
Anemometer	Wind speed	Above green roof	0.11 m/s	Met One 014A anemometer
Tipping-bucket rain gage	Precipitation	Weather station	Up to 1 in./h: ±1%	Texas electronic 525WS rain Gauge
Pyrgeometer	Incoming solar radiation	16 miles from green roof	<10%	CG3 pyrgeometer

VWC is the amount of moisture that the soil will hold; it is defined as the volume of water divided by the total volume of the sample, as shown in Eq. (4):

$$\mathrm{VWC} = \frac{V_{H_2O}}{V_{\mathrm{total}}} \tag{4}$$

Thus, the VWC values should be accurately predicted for precipitation events with little or no runoff, which was the case using Eq. (2).

Fig. 2 shows the measured precipitation and substrate water content for the first 8 days in July. In total, the first 19 days of July were utilized for the validation. These dates contain mostly clear sky conditions but they also contain a couple of precipitation events. Thus, the measured data set enabled the model validation under wet and dry conditions.

Unfortunately, the roof was instrumented with a net radiometer, but without a pyrgeometer, an instrument that measures incoming long wave radiation. Thus, the sky temperature was not measured directly. An indirect calculation of sky radiation is not accurate because it depends on roof surface temperature, emissivity and reflectivity. Early efforts to obtain sky temperatures from the net radiometer failed as shown in upcoming sections. This is a common situation in many green roof studies because building

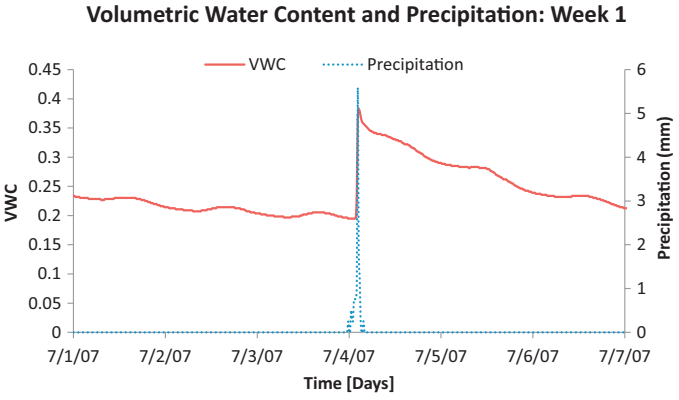

Fig. 2. Volumetric water content and precipitation measured during the first week of July.

field studies do not typically include a pyrgeometer. Most studies have typically used models to calculate the sky temperature. There are several models to calculate the sky temperature. The simplest model assumes that the sky temperature is equal to the air temperature, or it assume that the sky temperature is the same as the air temperature minus 20 °C (Jones, 1992). Other models use linear relationships between the sky temperature and the air temperature (Gaffin et al., 2005; Monteith and Unsworth, 2008) or they use nonlinear functions that depend on dew point temperature and time of the day (Duffie and Beckman, 1991) as shown in Equation 5 or required some knowledge of cloud cover (Swinbank, 1963; Cole, 1976; Martin and Berdahl, 1984). Models with cloud cover were not used in this study due to the lack of information regarding cloud cover. Therefore, this study initially used the clear sky model shown in Eq. (5), followed by actual long wave radiation data and Eq. (6). Thus the downward long wave radiation data ($\mathrm{Down}_{\mathrm{longwave,\,IR}}$) were obtained from a pyrgeometer located at the University of Chicago, approximately 16 miles from the green roof building test site to obtain sky temperature ($T_{\mathrm{sky,\,data}}$). Additional details on the pyrgeometer can be found in the literature (Barzyk and Frederick, 2008). In Eq. (6), σ is Stefan–Boltzmann constant, $5.64 \times 10^{-8}\,\mathrm{W/(m^2\,K^4)}$

$$T_{\mathrm{clear,\,sky}} = T_{\mathrm{air}} \cdot \left[0.711 + 0.56 \cdot \frac{dp}{100} + 0.73 \cdot \left(\frac{dp}{100}\right)^2 + 0.013 \cdot \cos\left(2 \cdot \pi \cdot \frac{\mathrm{Time}}{24}\right)\right]^{0.25} \tag{5}$$

$$T_{\mathrm{sky,data}} = \sqrt[4]{\frac{\mathrm{Down}_{\mathrm{longwave,\,IR}}}{\sigma}}\,\mathrm{Down}_{\mathrm{longwave,\,IR}} \tag{6}$$

Figs. 3 and 4 show the sky temperature calculated using Eq. (5) assuming clear sky conditions ($T_{\mathrm{clear,\,sky}}$), and Eq. (6) using incoming long wave radiation data ($T_{\mathrm{sky,\,data}}$). The results show that when calculating sky radiation assuming clear sky conditions, the simulated results can over or underpredict the actual sky temperature by up to 10 °C. This is because the model does not consider the cloud cover, and, therefore, the sky temperature can have different trends when compared to the real weather conditions. As a result, it is important to use real weather data when performing simulations with the green roof model.

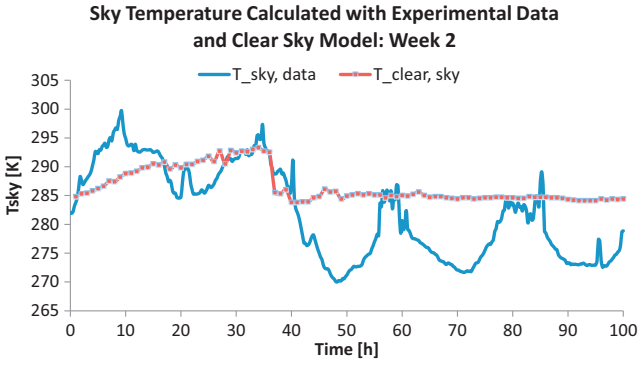

Fig. 3. Sky temperatures calculated using incoming long wave data ($T_{sky,\,data}$) and assuming clear sky conditions ($T_{clear,\,sky}$) during the second week of July.

3. Green roof model

Eqs. (7) and (8) express the energy balance around plants and the substrate for each layer on a green roof, assuming negligible plant thermal storage and metabolic rates. This approach decreases the number of equations needed to accurately solve the thermal transport through a green roof because only two equations are required instead of multiple equations for multiple layers used by other models (Table 1). The detailed development of this two-equation green roof model is available in the literature (Tabares-Velasco and Srebric, 2012).

$$R_{sh,\,abs,\,plants} = Q_{film,\,plants} + Q_{IR} \tag{7}$$

$$R_{sh,\,abs,\,substrate} = -Q_{IR} + Q_s + Q_{sub} + Q_{IR,\,sky} + Q_E \tag{8}$$

In Eq. (7), $R_{sh,\,abs,\,plants}$ is the absorbed solar radiation by the plants; Q_{IR} is the radiative heat transfer between the plant layer and the top substrate layer; and $Q_{film,\,plants}$ represents the heat transfer between plants and the surrounding environment by means of latent heat flux (transpiration), convective and radiative heat transfer. In Eq. (8), $R_{sh,\,abs,\,substrate}$ is the absorbed solar radiation by substrate underneath the plants, Q_{IR}, is the long wave radiation between the plant layer and the top substrate layer, Q_S is the convective heat transfer between the top substrate layer and the surrounding air, Q_{sub} is the conductive heat flux through green roof substrate, and $Q_{IR,\,sky}$ is the long wave radiation exchanged between the substrate and sky.

The conductive heat transfer through the green roof substrate is calculated with Eq. (9), where the conduction through non-vegetated and vegetated sections of the roofs is considered. The next heat transfer mechanism to be considered is convection. The convective heat transfer coefficient was originally developed for horizontal flat plates (Wang, 1982; Tabares-Velasco and Srebric, 2012). Thus, a coefficient (β) was added in order to account for the green roof roughness in Eq. (10). The value for β was initially set to 1.5 (Tabares-Velasco and Srebric, 2012), but later modified to 3 for vegetated sections of the green roof and 2.1 for the section of the roof without plants. The new coefficients are based on previous research for convection heat on roofs (Clear et al., 2003).

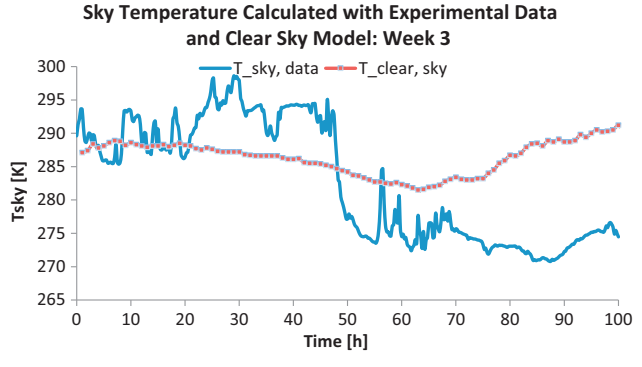

Fig. 4. Sky temperatures calculated using incoming long wave data ($T_{sky,\,data}$) and assuming clear sky conditions ($T_{clear,\,sky}$) during the third week of July.

$$Q_{sub} = \sigma_f Q_{in,\,sub,\,plants} + (1-\sigma_f) Q_{in,\,sub,\,bare} \tag{9}$$

$$Q_{convection,\,plants} = \beta \times LAI \times h_{conv}(T_{plants} - T_{air}) \tag{10}$$

Where LAI is the leaf area index [(leaf area)/(substrate surface)], h_{conv} is convective heat transfer coefficient, and T_{plants} and T_{air} are the temperatures for plants and surrounding air, respectively.

This model was previously validated with quasi-steady state data collected in the "Cold Plate" apparatus (Tabares-Velasco and Srebric, 2012). Thus, heat transfer though the substrate was successfully calculated using only conduction heat transfer neglecting any thermal storage. However, earlier efforts with the current experimental data set demonstrated the need to properly model the thermal mass of the substrate. Thus, in this present study, the thermal mass of the substrate is added using conduction transfer functions (CTF). CTFs are typically used in building energy simulation programs that calculate the annual energy consumption of buildings. They have been widely used because they relate the current conduction heat fluxes to current and past surface temperatures and past heat fluxes using X, Y, Z and φ coefficients that depend on the wall or surface properties and time step used the heat flux calculations (ASHRAE, 2005). This method greatly simplifies the problem when compared with the finite differential method because no iterations are needed and there is no need to calculate inner node temperatures. However, CTFs only allow the use of constant physical–thermal properties, thus any changes in the thermal conductivity, density and specific heat of the substrate due to the change in water content will not be considered in this analysis. The transfer functions used in this study were obtained from EnergyPlus, a building energy simulation program using a time step of 15 min and are shown in Table 3. These values were obtained using green roof substrate thermal conductivity equal to 0.25 W/(m K), density of 850 kg/m^3 and specific heat of 1400 kJ/(kg °C). Due to the limitations of CTFs in only allowing for the bulk material properties, all material property values were kept constant including the conductivity of 0.25 W/(m K), which reflects an average VWC of 0.18. However, actual VWC varied from 0.15 to 0.40.

For the evapotranspiration calculation, Monteith introduced an aerodynamic and surface resistance to heat and mass (vapor) transfer that is now widely used (Hillel, 1998). This two-equation green roof model followed the vapor pressure deficit (VPD) approach, using Eqs. (11) and (12) to calculate the evapotranspiration for substrate layer with plants ($Q_{T,p}$) and without plants ($Q_{E,b}$) separately.

$$Q_{T,\,p} = LAI \frac{\rho C_p}{\gamma(r_s + r_a)}(e_{s,\,plants} - e_{air}) \tag{11}$$

$$Q_{E,\,b} = \frac{\rho C_p}{\gamma(r_{so} + r_{a,\,bare})}(e_{s,\,soil,\,b} - e_{air}) \tag{12}$$

where $e_{s,\,plants}$ and $e_{s,\,soil,\,b}$ are the vapor pressure at the evaporative surface for the roofs with and without plants, e_{air} is the vapor pressure of the air. Furthermore, r_s is stomatal resistance to mass transfer, r_a and $r_{a,\,bare}$ are the aerodynamic resistance to mass transfer. γ is the psychrometric constant and equals to $C_pP/0.622i_{fg}$, in which i_{fg} is the enthalpy of vaporization, and P is the atmospheric pressure (Tabares-Velasco and Srebric, 2012; Hillel, 1998). Stomatal resistance is variable as it depends on the plant type and environmental variables such as solar radiation, vapor pressure, temperature and water content in the soil and plant. The

Table 3
CTF coefficients used for solving transient conductive heat transfer through the substrate.

CTF	*X*-exterior (W/(m^2 K))	*Y*-cross (W/(m^2 K))	*Z*-interior (W/(m^2 K))	Flux (W/m^2)
0	14.6618	6.85E−05	4.57384	
1	−30.9672	4.38E−03	−11.2695	1.757663
2	21.15352	1.65E−02	10.07377	−0.97166
3	−5.22433	1.04E−02	−3.97879	0.194661
4	0.419112	1.32E−03	0.675899	−1.34E−02
5	−1.02E−02	2.99E−05	−4.34E−02	2.97E−04
6	6.79E−05	7.56E−08	9.36E−04	−1.87E−06
7	−3.09E−10	3.34E−12	−5.84E−06	8.54E−12
8	1.96E−14	−3.56E−15	1.03E−11	−1.31E−15

model used in this study takes into account all of these factors using a multiplicative approach. The multiplicative functions were selected after comparing several stomatal functions against experimental data from the "Cold Plate" apparatus (Tabares-Velasco and Srebric, 2012). Thus, even though substrate thermal conductivity was assumed constant, the model did account for changes in evapotranspiration due to substrate VWC.

4. Validation results and discussion

Verification and validation are important components of modeling. The existing literature presents several definitions for validation. This study uses the definition by ERCOFTAC that defines validation as "a procedure to test the extent to which the model accurately represents reality" (ERCOFTAC, 2000). Thus, in this study, the validation presents a procedure to demonstrate that the green roof model is capable of predicting an actual green roof performance. The inputs to the green roof model for the validation include the following parameters:

- Roof top wind speed (m/s)
- Solar radiation (W/m^2)
- Air temperature (°C)
- Relative humidity, RH (%)
- Substrate water content (m^3/m^3)
- Down long-wave radiation from the sky (W/m^2)

Early tests with the green roof model using Eq. (5) showed days with an excellent agreement between results and experimental data for the net radiation, and days with only fair agreement. This bias was probably due to clouds not accounted for the clear sky model. Therefore, in the next step, this study used actual incoming long-wave radiation data from the pyrgeometer. Once all the data were input into the model, the variables that needed to be analyzed were: (1) substrate temperature, (2) heat flux through the green roof, and (3) net radiation.

Additional green roof specifications that remain constant for all simulations were (1) LAI equal to 1.5, (2) substrate thickness equal to 0.075 m, (3) minimum stomatal resistance equal to700 s/m, based on previous work with similar plants (Tabares-Velasco and Srebric, 2012), (4) plants extinction coefficients of 0.7–0.83 and σ_f equal to 0.75 based on input from the green roof company that installed and monitored the roof. Additionally, the lower boundary conditions were set with the temperature measurements from the thermocouples located underneath the drainage layer as shown in Fig. 1. In this way, only the interaction between the green roofs and the environment were investigated.

4.1. Substrate top temperature

The substrate top temperature is an important parameter to indicate thermal performance of a green roof because it is directly proportional to the heat flux transferred through the roofing layers in steady or quasi steady state conditions but not necessary for a roof with dynamic conditions and large thermal mass. Figs. 5 and 6 show, on the left axis: (1) the measured green roof substrate top temperature ($T_{sub,\,data}$), (2) simulated substrate top temperature for a green roof covered with plants ($T_{sub,\,top,\,plants}$), (3) and a bare green roof without plants ($T_{sub,\,top,\,bare}$) for two different time periods in July, the second and third week. Figs. 5 and 6 also show, on the right axis, the volumetric water content of the substrate (VWC). The bare and covered substrate temperatures were calculated because they were needed to calculate the overall conductive heat transfer through the green roof. Green roofs typically have areas that are fully covered and areas that are not completely covered by plants.

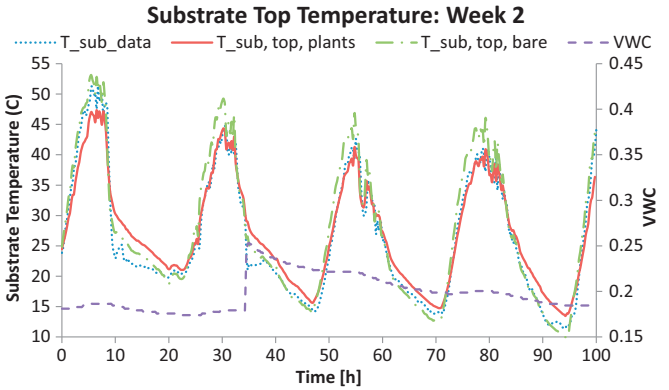

Fig. 5. Substrate top temperature measured data ($T_{sub,\,data}$), calculated substrate top temperatures for bare substrate roof ($T_{sub,\,top,\,bare}$), and calculated substrate top temperatures for substrate covered by plants ($T_{sub,\,top,\,plants}$) during the second week of July.

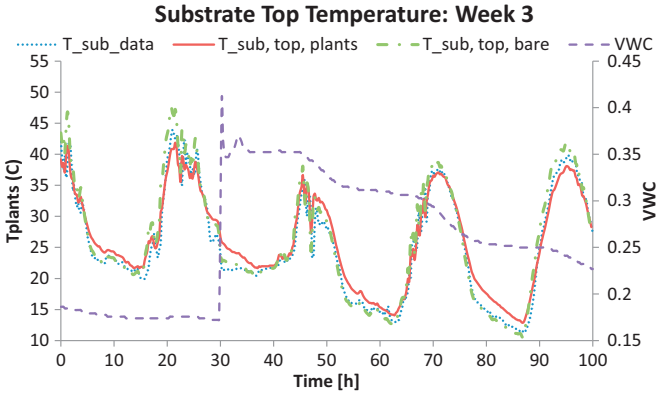

Fig. 6. Substrate top temperature measured data ($T_{sub,\,data}$), calculated substrate top temperatures for bare substrate roof ($T_{sub,\,top,\,bare}$), and calculated substrate top temperatures for substrate covered by plants ($T_{sub,\,top,\,plants}$) during the third week of July.

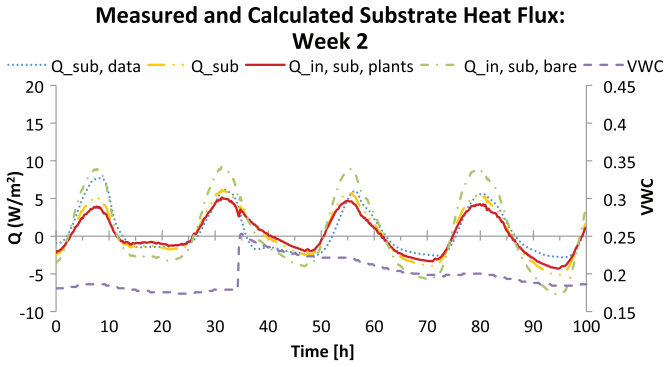

Fig. 7. Substrate heat flux data ($Q_{sub,\ data}$), calculated combined heat fluxes (Q_{sub}), calculated heat fluxes for bare substrate roof ($Q_{in,\ sub\ bare}$) and calculated heat fluxes for green roof covered by plants ($Q_{in,\ sub,\ plants}$) during the second week of July.

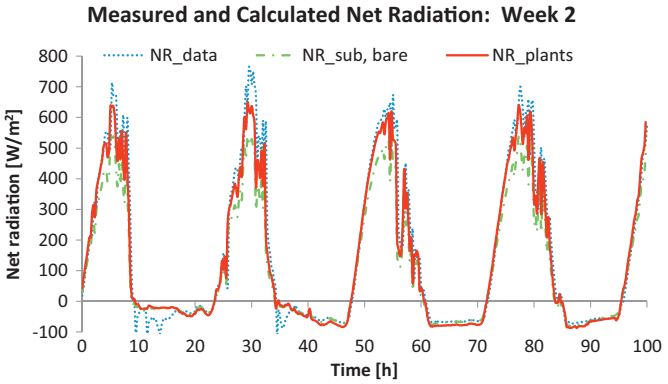

Fig. 9. Measured net radiation (NR_{data}), and calculated net radiation for bare substrate roof ($NR_{subl,\ bare}$) and for green roof covered with plants (NR_{plants}) during the second week of July.

Overall, the results in Figs. 5 and 6 show that the model accurately predicted the substrate top temperature of the green roof. Among the two simulated temperatures, $T_{sub,\ top,\ bare}$ is the highest, which suggests that the plants of the green roofs reduced the substrate top temperature and that the thermocouples were probably covered by plants. The results also show the highest disagreement between experimental data and simulated results right after a rain event, probably because substrate temperature might be lowered by rain having a lower temperature than the substrate. Rain events can be identified, in Figs. 5 and 6, by a sudden increase in VWC. The sudden increase in VWC changes the substrate thermal conductivity drastically, and unfortunately at this stage this dependency was not modeled. However, other variables that depend on VWC were simulated, such as the following variable: (1) substrate reflectivity, (2) substrate resistance to evaporation and (3) plants resistance to transpiration. Furthermore, substrate temperatures of the green roof and thermal conductivity are two key variables to calculate heat transfer through the substrate.

4.2. Heat flux through the green roof substrate

The heat flux through the substrate defines the thermal loads from the roofing layers. Figs. 7 and 8 show the measured substrate heat flux ($Q_{sub,\ data}$), calculated heat flux for the green roof section covered with plants ($Q_{in,\ sub,\ plants}$), calculated heat flux for bare green roof section ($Q_{in,\ sub\ bare}$) and combined heat flux (Q_{sub}) for the same 2 weeks as Figs. 7 and 8. The combined heat flux (Q_{sub}) is calculated using Eq. (9). $Q_{in,\ sub,\ plants}$ and $Q_{in,\ sub\ bare}$ are the calculated total heat fluxes for the area of roof with plants and for the area of roof without plants using the same CTFs shown in Table 3. The

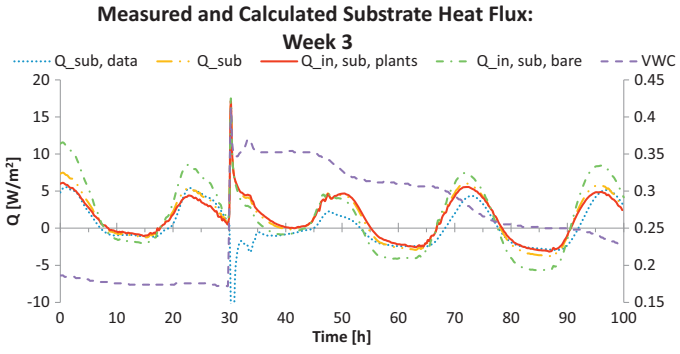

Fig. 8. Substrate heat flux data ($Q_{sub,\ data}$), calculated combined heat fluxes (Q_{sub}), calculated heat fluxes for bare substrate roof ($Q_{in,\ sub\ bare}$) and calculated heat fluxes for green roof covered by plants ($Q_{in,\ sub,\ plants}$) during the third week of July.

model predicts lower heat fluxes for the green roof area with plants than the heat fluxes for the green roof area without plants. Since the entire roof includes areas with plants and areas without plants, the total measured substrate heat flux is between $Q_{in,\ sub,\ plants}$ and $Q_{in,\ sub\ bare}$. Unfortunately, in the current green roof design it was not possible to measure both heat fluxes individually. The model tends to predict most of the peak heat fluxes except for a couple of days immediately after a rain event causing a rapid change in the substrate thermal properties, not considered in this model due to the limitations of CTFs. This particular disagreement is strongest during the third week of July as presented in Fig. 8 when time is around 30 h. This day had the strongest precipitation event in the month and the substrate was completely saturated (VWC around 0.40), so the measured and calculated heat fluxes show a similar trend but with opposite sign. More importantly, in that event there was runoff during and immediately after the rain which would reflect as heat removed into the runoff water. This effect is not part of the model.

4.3. Net radiation

Net radiation is also a very important parameter as it combines downward and upward solar and long-wave radiation and represents the major incoming heat flux. Net radiation depends on several variables such as incoming solar and long-wave radiation, green roof reflectivity and temperature. Because the green roof was not homogeneous (bared and covered areas happen naturally and with time the bared sections will decrease), the net radiometer located 1.2 m above the green roof was measuring the average net radiation on the green roof. Figs. 9 and 10 show the measured net radiation (NR_{data}) versus the simulated net radiation for the bare substrate roof ($NR_{sub,\ bare}$) and for the substrate covered with plants (NR_{plants}). In particular, the radiation sensor in the weather station was mounted just slightly above the plant height. For most cases, the model for the green roof covered with plants calculated similar net radiation to the measured data. These results were consistent with the overall performance of the model for green roof with plants when compared with the measured surface temperatures and heat fluxes. Moreover, the discrepancies were consistent with the discrepancies shown in Figs. 9 and 10 that follow trends defined by the green roof top surface. This connection between the top surface temperatures and net radiation is due to the fact that the net radiation strongly depends on the substrate top temperature. Thus, when the top temperature is accurately simulated, the net radiation is also accurately simulated.

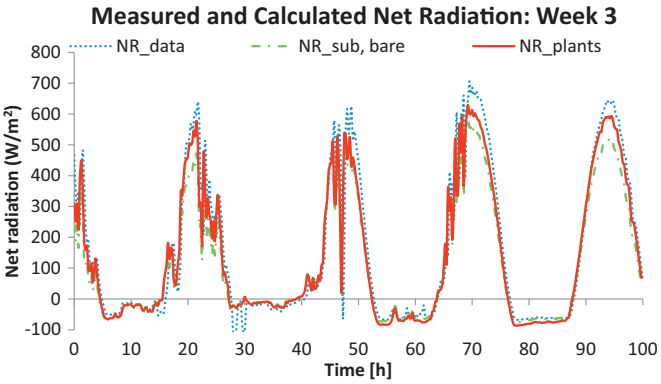

Fig. 10. Measured net radiation (NR_{data}), and calculated net radiation for bare substrate roof ($NR_{subl,\ bare}$) and for green roof covered with plants (NR_{plants}) during the third week of July.

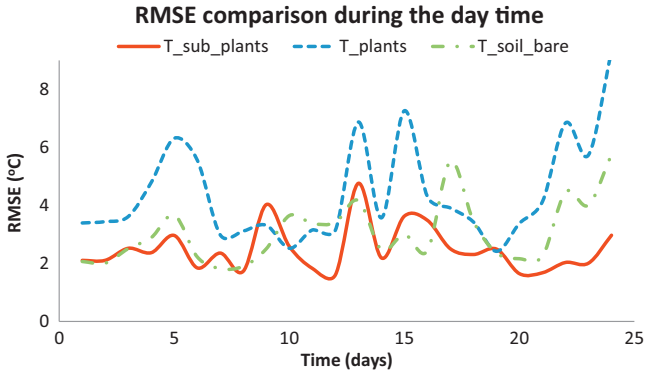

Fig. 11. RMSE for top substrate temperatures calculated by the model without plants ($T_{sub,bare}$), top substrate temperatures covered by plants (T_{sub_plants}) and plant surface temperatures (T_{plants}) during day time.

Table 4
Green roof model performance evaluation based on root mean square error (RMSE)and normalized root mean square error (NRMSE).

	RMSE	NRMSE
$T_{sub,\ top,\ plants}$ (°C)	2.36	0.06
$T_{sub,\ top,\ bare}$ (°C)	2.59	0.06
T_{plants} (°C)	3.74	0.09
NR_{bare} (W/m^2)	85.48	0.09
NR_{plants} (W/m^2)	67.07	0.07
Q_{sub} (W/m^2)	1.44	0.10

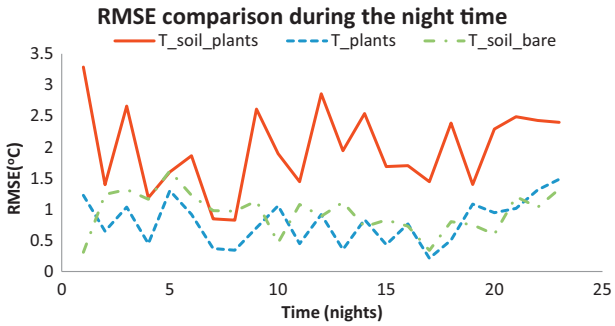

Fig. 12. RMSE for top substrate temperatures calculated by the model without plants ($T_{sub,bare}$), top substrate temperatures covered by plants (T_{sub_plants}) and plant surface temperatures (T_{plants}) during night time.

4.4. Evaluation of model performance

The green roof model performance was evaluated based on the comparisons of the measured and calculated surface temperatures, heat fluxes and net radiation as shown in Figs. 5–10. In addition, this study validated the proposed green roof model based on the root mean square error (RMSE), and normalized root mean square error (NRMSE) shown in Table 4. RMSE and NRMSE were all calculated using the 15 min experimental and calculated data. Overall, the sample size or number of values used to calculate RMSE and NRMSE were more than 2000 for each variable. For example, in Table 4 RMSE of $T_{sub,\ top,\ plants}$ was calculated using the experimental data that measured green roof substrate top temperature and the data from the model that calculated the substrate top temperature for a green roof covered with plants. These calculations do not include data when there was precipitation, since at this point the model does not take precipitation into account. For comparative purposes, RMSE and NRMSE are calculated for the surface temperatures of the bare substrate area, surface temperatures of the covered substrate area and surface temperatures of the plants. These values were calculated using the measured green roof surface temperatures. From the three surface temperatures, plant temperature resulted in the highest disagreement. This is not surprising, as the measured plant surface temperatures were probably the temperatures of the substrate covered by the plants. Thus, the experimental data did not include any plant temperatures. Table 4 indicates that most of the heat and mass transfer was predicted accurately and that the best surface temperature agreement was achieved when the plants shading and shielding are included in the calculations of the substrate surface temperature.

The RMSE shown in Table 4 are similar to the results in a previous study using this model (Tabares-Velasco and Srebric, 2012), except the RMSE and NRMSE of the substrate temperature of the green roof, which were higher in the present validation study. Table 4 shows the result comparison from the two different validation efforts (see Table 5).

Figs. 11 and 12 show the RMSE comparisons during the day time and night time. From these figures, the substrate temperature RMSE of the green roof (T_{sub_plants}) is the smallest compared to the RMSE to top substrate temperature covered by plants (T_{sub_plants}) and plant surface temperatures (T_{plants}) during day time during the day as shown in Fig. 11. However, the substrate temperature RMSE of the green roof is the highest compared to the RMSE to top substrate temperature covered by plants (T_{sub_plants}) and plant surface temperatures (T_{plants}) during the night as shown in Fig. 12. This suggests that the long-wave radiation exchange between the sky and the substrate could be underestimated in the model, as the biggest difference occurs during the night when the long wave radiation has a significant role in the heat transfer. This could also be due to the selected extinction coefficient of 0.83 or selected LAI.

Table 5
Comparison of root mean square error (RMSE) and normalized root mean square error (NRMSE) from two different validation efforts.

	RMSE		NRMSE	
	Current experiment	Tabares-Velasco and Srebric (2011)	Current experiment	Tabares-Velasco and Srebric (2011)
$T_{sub,\ top}$ (°C)	2.36	2	0.06	0.07
Q_{sub} (W/m^2)	1.44	4	0.10	0.21

5. Discussion

Previous green roof models have validated thermal models based mainly on substrate surface temperature. Single surface temperature validation is not enough to guarantee that a model is correctly simulating evapotranspiration, convection, radiation and conduction, due to the complexivity and nonlinearity of the physical processes involved in the heat and mass transfer in green roofs. Thus, the proposed model is a result of:

1. Previous detailed steady state laboratory validation against evapotranspiation, convection, conduction and surface temperatures under different environmental condditions (Tabares-Velasco and Srebric, 2011, 2012).
2. Dynamic validation under outdoor conditions after detailed steady state validation have shown the model produces accurate and reliable results for variables such as evapotranspiration.

Based on the agreement shown in these studies, this is the final step in demonstrating how accurately the model performs during summer conditions. Users of the model now have a fully validated green roof model. This set of studies also produced and recommeded inputs needed for simulating green roofs such as LAI, stomatal resistance, and substrate resistance to evaporation. The next step will be the full implemenation into a building energy simulation program such as EnergyPlus.

6. Conclusions

In this study, a heat and mass transfer model was validated using field data from a green roof installed on a commercial roof in Chicago. The validation also used on-site weather data that included long-wave radiation, a variable that in many practical situations is not known. The validation consisted of comparing surface temperatures, heat fluxes through the roof, and net radiation measured on a green roof to the values predicted by the green roof model.

The results show that the model yields surface temperatures similar to the experimental data, although the model tends to underestimate the green roof heat fluxes in some cases. Possible reasons for the underestimation are the constant thermal conductivity limitation in the model, and lack of accurate information on the green roof LAI and coverage. The results also show the importance of correctly modeling the plants as the closest agreement of the data and the model was obtained when plant coverage was considered. In addition, the results show that performance of simulated net radiation depends on the performance of simulated substrate top temperature because of their interdependence.

In order to further analyze the performance of the model, the root mean square error (RMSE), and normalized root mean square error (NRMSE) were calculated for surface temperatures, heat fluxes through the roof, and neat radiation. The RMSE for surface temperatures was compared during the day time and night time, showing better agreement during the day than during the night.

Overall, the model is fully validated after going through two different valiation tests: a laboratory quasity-steady test and a transient outdoor test. To the best of the authors' knowlewdge, this is the only model that has been validated using this detailed approach. Thus, the authors feel confident of the model accuracy when used for modeling extensive green roof performance under summer conditions except in precipitation events when runoff is removing heat and/or rain tempeature is significantly lower than roof tempeature. These issues will be investigated in future research as will the performance of the model when variable properties of the substrate are included, and the model will be incorporated into EnergyPlus.

References

Alexandri, E., Jones, P., 2007. Developing a one-dimensional heat and mass transfer algorithm for describing the effect of green roofs on the built environment: comparison with experimental results. Build. Environ. 42 (8), 2835–2849.

ASHRAE, 2005. ASHRAE Handbook Fundamentals. ASHRAE, Atlanta.

Barzyk, T.M., Frederick, J.E., 2008. A semiempirical microscale model of the surface energy balance and its application to two urban rooftops. J. Appl. Meteorol. Climatol. 47 (3), 819–834.

Clear, R.D., Gartland, L., et al., 2003. An empirical correlation for the outside convective air-film coefficient for horizontal roofs. Energ. Buildings 35 (8), 797–811.

Cole, R.J., 1976. Direct solar radiation data as input into mathematical models describing the thermal performance of buildings, I. A review of existing relationships which predict the direct component of solar radiation. Build. Environ. 2, 173–179.

Del Barrio, E., 1998. Analysis of the green roofs cooling potential in buildings. Energ. Buildings 27 (2), 179–193.

Duffie, J.A., Beckman, W.A., 1991. Solar Engineering of Thermal Processes. Wiley, New York.

ERCOFTAC, 2000. The ERCOFTAC Best Practice Guidelines for Industrial Computational Fluid Dynamics. ERCOFTAC Interest Group on Quality and Trust in Industrial CFD, ERCOFTAC Coordination Centre STI-LMF-EPFL, Lausanne, Switzerland, p. 95.

Gaffin, S., Rosenzweig, R.C., et al., 2005. Energy balance modeling applied to a comparison of green and white roof cooling efficiency. In: Third Annual International Greening Rooftops for Sustainable Communities, Conference, Awards & Trade Show, Washington, DC, pp. 15–27.

Gregoire, B.G., Clausen, J.C., 2011. Effect of a modular extensive green roof on stormwater runoff and water quality. Ecol. Eng. 37 (6), 963–969.

He, H., 2010. Simulation of thermodynamic transmission in green roof ecosystem. Ecol. Model. 221 (24), 2949–2958.

Hillel, D., 1998. Environmental Soil Physics. Academic Press, San Diego.

Johnston, A., 2007. Annual green roof industry survey shows 24 percent growth in North American. Green Roof Infrastruct. Monit. 9 (2), 28.

Jones, H.G., 1992. Plants and Microclimate. Cambridge University Press, Cambridge.

Justyna, C.B., 2010. Green roof performance towards management of runoff water quantity and quality: a review. Ecol. Eng. 36 (4), 351–360.

Lazzarin, R.M., Castelloti, F., Busato, F., 2005. Experimental measurements and numerical modelling of a green roof. Energ. Buildings 37 (12), 1260–1267.

MacIvor, J.S., Lundholm, J., 2011. Performance evaluation of native plants suited to extensive green roof conditions in a maritime climate. Ecol. Eng. 37 (3), 407–417.

Martin, M., Berdahl, P., 1984. Characteristics of infrared sky radiation in the United States. Solar Energy 33 (3–4), 321–336.

Miller, C., Narejo, D., 2005. State of the green roof industry in the United States. Geo-Frontiers, 4057–4064.

Molineux, C.J., Fentiman, C.H., et al., 2009. Characterizing alternative recycled waste materials for use as green roof growing media in the U.K. Ecol. Eng. 35 (10), 1507–1513.

Monteith, J.L., Unsworth, M.H., 2008. Principles of Environmental Physics. Academic Press, London.

Nayak, J.K., Srivastava, A., Singh, U., Sodha, M.S., 1982. Relative performance of different approaches to the passive cooling of roofs. Build. Environ. 17 (2), 145–161.

Peck, S., 2011. Annual Green Roof Industry Survey.

Perino, M., Serra, M., 2003. Filippi, Monitoraggio del comportamento termico di un tetto verde: primi risultati sperimentali. In: Congresso nazionale ATI 2003, Padova, Italy, pp. 1863–1872.

Sailor, D.J., 2008. Thermal property measurements for ecoroof soils common in the western U.S. Energ. Buildings 40 (7), 1246–1251.

Snodgrass, E.C., 2006. Green Roof Plants: A Resource and Planting Guide. Timber Press, Portland.

Swinbank, W.C., 1963. Long-wave radiation from clear skies. Quarterly Journal of the Royal Meteorological Society 9 (381), 339–348.

Tabares-Velasco, P.C., Srebric, J., 2009a. The role of plants in the reduction of heat flux through green roofs: laboratory experiments. ASHRAE Trans. 115 (2), 793–802.

Tabares-Velasco, P.C., Srebric, J., 2009b. Heat fluxes and water management of a green and brown roof: laboratory experiments. In: Seventh Annual International Greening Rooftops for Sustainable Communities Conference, Atlanta, GA, June.

Tabares-Velasco, P.C., Srebric, J., 2011. Experimental quantification of heat and mass transfer process through vegetated roof samples in a new laboratory setup. Int. J. Heat Mass Transfer 54 (25-26), 5149–5162.

Tabares-Velasco, P.C., Srebric, J., 2012. A heat transfer model for assessment of plant based roofing systems in summer conditions. Build. Environ. 49, 310–323.

Takebayashi, H., Moriyama, M., 2000. Surface heat budget on green roof and high reflection roof for mitigation of urban heat island. Build. Environ. 42, 2971–2979.

Wang, X.A., 1982. An experimental study of mixed, forced, and free convection heat transfer from a horizontal flat plate to air. J. Heat Transfer 104 (1), 139–144.